

Elastowave: Localized Tactile Feedback in a Soft Haptic Interface via Focused Elastic Waves

Gregory Reardon¹, Nikolas Kastor³, Yitian Shao², and Yon Visell^{1,2}

Abstract—It is challenging to engineer programmable tactile displays to match human haptic abilities. Such displays are often composed of elements whose stiffness contrasts greatly with the softness of many natural materials. Emerging soft material technologies hold promise for their ability to conform to many objects, including the human body. However, rendering localized feedback from soft haptic devices remains challenging. Here, we present the Elastowave, a soft tactile interface that provides localized tactile feedback via a soft, compliant surface. We achieve this by focusing elastic wave fields generated by a compact array of remotely-positioned actuators. Our method is based on new variations of time-reversal focusing techniques for elastodynamic waves. Our system can provide dynamic, single- or multi-point localized tactile feedback with centimeter-scale resolution across a deformable interface with an area of 175 cm². The sizeable displacements of the focused tactile signals enable them to be easily felt, as our experiments show. This work could enable the design of a multitude of new soft tactile interfaces in areas such as creative computing, product design, and augmented reality.

I. INTRODUCTION

Haptic engineering aims at creating technologies that address the sense of touch. Most haptic devices are composed of hard, rigid elements [1], [2], [3]. Even with careful engineering, it is difficult to convincingly render experiences of touching many natural, soft surfaces using such devices. Technologies that could reproduce such experiences would hold great value in product design, creative computing, ergonomics, health, and virtual and augmented reality applications. An alternative is to design haptic interfaces from soft materials. The term “soft” has been employed in different ways in the literature [4]. Here, we use it to refer to materials that are deformable, like soft tissues in the human body.

Emerging research in haptics aims to create soft material technologies for use in interfaces that can deliver programmable tactile feedback. Other advantages of such technologies include their resilience and compliance [5], which can enable them to conform to diverse objects and surfaces, including the human body. Today, however, few soft material technologies can render localized tactile feedback as accurately as conventional devices, such as variable friction touch screens or arrays of rigid actuators. A further challenge in realizing soft display technologies for haptics is that soft materials are continua with infinitely many mechanical degrees of freedom, few of which can be controlled

in practice. Overcoming these challenges could enable a wide range of new products and experiences, such as soft tactile touch pads for expressive computing, wearable soft tactile displays, soft tactile communication interfaces, or programmable soft control interfaces for automotive, home, or work environments, among many other possibilities.

Various approaches to the design of soft tactile interfaces have been previously explored, based on pneumatically or hydraulically actuated soft media [6], [7], granular jamming [8], electrostatic actuation [9], [10], electromagnetic polymer devices [11], and other approaches, including many based on smart material technologies. For a recent review, see [12]. Despite recent advances in soft haptics, it has proved extremely challenging to engineer integrated soft actuator arrays that are practical to fabricate, manufacture, and operate, that achieve sufficient density to supply distributed, localized feedback, that are reasonably resilient to deformations, that are stable and reliable, and that can be integrated in soft media. Hybrid approaches, in which conventional actuators (such as motors) are integrated in soft materials, introduce other problems, such as thermal regulation and mechanical coupling artifacts that cause tactile feedback to be diffused throughout the medium. Here, we present a new method of designing a soft tactile interface that exploits mechanical transmission in soft media in order to allow the actuators to be positioned away from the active area of the device. Their removal also allows the device interface to be greatly deformed, stretched, or bent without breaking (Fig. 1). While other devices have used soft layers to remotely transmit tactile signals [13], they have offered little control over the localization of the feedback.

Our device, which we refer to as Elastowave, provides localized tactile feedback by focusing elastic wave fields generated by a compact array of remotely positioned actuators. It achieves this via new variations of time-reversal focusing techniques for elastodynamic waves [14]. It can provide single- or multi-point localized tactile feedback with centimeter-scale resolution across a soft, deformable interface. Unlike other focusing methods, such as wave field synthesis [15], this method does not require parameters of an analytical model of wave transmission in the medium to be identified. Time-reversal methods have previously been used in order to localize tactile feedback via flexural waves in rigid plates [16], [17]. (Similar methods have been explored for coarsely focusing tactile feedback via ultrasonic waves in the skin [18].) Elastic waves are vector fields, and possess many more degrees-of-freedom than flexural waves in rigid plates. Due to the rigidity of such plates, time-reversal

¹ Media Arts and Technology Program, University of California, Santa Barbara, California. Contact Email: reardon@ucsb.edu

²Department of Electrical and Computer Engineering, University of Santa Barbara, Santa Barbara, California.

³California NanoSystems Institute, University of California Santa Barbara, Santa Barbara, California.

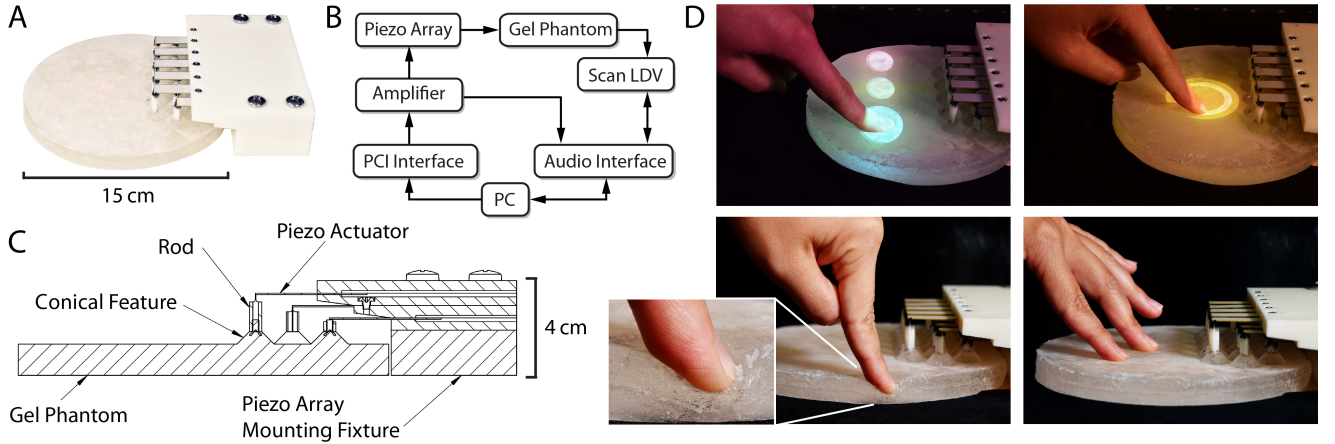


Fig. 1: A) Elastowave is a soft tactile interface. It provides localized, multi-point tactile feedback via focused elastic waves generated by a compact actuator array. B) The control system comprises a PC running custom software, and other hardware. A scanning LDV captures dynamic wave fields on the surface. C) The piezoelectric cantilevers actuate the medium at raised conical features that aid impedance matching. D) Users feel dynamic, localized multi-point tactile feedback. Sensing and visual feedback may be added to enable multimodal interaction (upper left: tactile buttons, upper right: continuous dial).

focusing of flexural waves yields small amplitude motion at near-ultrasonic frequencies; the mechanisms that allow such waves to be felt are not fully understood [17]. The soft mechanics of our device enable us to generate far larger displacements than are produced by flexural wave focusing or via mid-air haptics with focused ultrasound [18]. The lower propagation speeds of elastic waves in soft media also enable our device to produce localized tactile feedback for which nearly all of the energy is concentrated in a frequency range, near 200 Hz, that is highly salient to tactile perception. The low mechanical impedance of the medium ensures that this energy is transmitted to the skin more efficiently than is possible with a rigid display made from hard materials. As our results show, these properties ensure that the feedback from our device is easy to perceive. While our device does not yet integrate sensing, a wide array of sensing methods could be integrated, including optical, resistive, capacitive, or acoustic sensing techniques. We have prototyped simple interactive applications by combining the Elastowave with a camera and projector system. Many other combinations with sensing and visual feedback are possible.

In the next sections, we describe the design and fabrication of the Elastowave, and methods for rendering localized tactile feedback via focused elastic waves. Because our method is data-driven rather than model based, other materials, actuators, array configurations, and geometries could be used. We present empirical characterizations of the device based on full-field optical vibrometry experiments. We present the implementation of our focusing method, and empirical evaluations of results for single- and multi-point focusing of dynamic tactile feedback. In a perceptual study, we demonstrate that users can easily perceive localized single- or multi-point tactile feedback from our device. We conclude with a discussion of the results and new research opportunities and applications suggested by this work.

II. SOFT TACTILE INTERFACE DESIGN

Our device consists of a soft, deformable tablet-like interface that provides localized, time-varying tactile feedback at dynamically programmable locations (Fig. 1A). It consists of a soft elastomer plate of approximately cylindrical shape, with dimensions 15 cm diameter and 1 cm thickness. The device provides localized tactile feedback via spatially and temporally focused waves excited by an array of remotely positioned actuators. The wave focusing technique is described in Sec. IIIB, and the implementation is described in Sec. V.

We selected the material to approximately match the mechanical impedance of human skin in order to maximize the efficiency of vibration energy transmission to the finger. If the complex impedance of the medium in the Laplace domain is $Z_m(s)$ and that of a user's finger is $Z_f(s)$, the reflected energy of vibrations impinging on the finger is proportional to the reflection coefficient, $\Gamma = (Z_f - Z_m)/(Z_f + Z_m)$, which is minimized for $Z_m \approx Z_f$. We achieved this by fabricating the plate from solid, synthetic medical gel (Gelatin #2, Humimic, USA, mass density: 925 kg/m³), whose mechanical properties are designed to be similar to human skin. The tablet is actuated by 16 piezoelectric bimorph cantilevers (model SMBA4510T05M, Steminc., USA) integrated in a custom 3D printed fixture and positioned in three rows near one side of the medium. The actuators are driven by independent, time-varying bipolar signals supplied by a multichannel, piezoelectric amplifier (PD32, Piezodrive, Australia) driven via analog signals from a digital-to-analog converter (National Instruments, USA, 12 bits, sample rate 10 kHz) that is driven using customized software (Fig. 1B).

The piezo actuators supplied bipolar driving forces to the medium via rigid rods that were connected to the cantilevers by way of compliant hinges. The hinges enabled the driving rods to displace without imparting a moment to the soft

medium. The rods were attached to over-molded threaded inserts embedded in soft, raised conical features whose shape reduced the impedance mismatch between the actuators and gel medium (Fig. 1C). To ensure a compact design, the actuators were positioned in three rows (5, 6, and 5 each), with successive rows offset in height and position.

We fabricated the tablet using a multi-step casting process. First, we produced a 3D mold with inverse conical features by laser cutting, machining, and stacking 8 mm polycarbonate plates. After treating the mold surface with a releasing agent, we dispersed a thin layer of reflective glass microbeads in the inverted top of the mold to facilitate the laser vibrometry measurements (Sec. IV). Threaded posts were then placed at each actuation site to be over-molded as inserts at the tip of the conical features. The rods were screwed to these posts during assembly. We melted the synthetic gel in the mold in a laboratory oven and allowed the gel to cool. We then demolded the gel and mounted it on a base while aligning the rods with the actuator array. We affixed the free ends of the piezoelectric bimorphs to the rods using a compliant room-temperature-vulcanized rubber adhesive.

III. FOCUSING VISCOELASTIC WAVES

The driven response of an idealized (homogeneous, isotropic) elastic medium to a driving force field $\mathbf{f}(\mathbf{x}, t)$ is described by a time-varying vector displacement field, $\boldsymbol{\xi}(\mathbf{x}, t)$, satisfying (for small amplitudes) a linear wave equation,

$$L \boldsymbol{\xi}(\mathbf{x}, t) = \mathbf{f}(\mathbf{x}, t), \quad (1)$$

$$\text{where } L = -\rho \frac{\partial^2}{\partial t^2} + \mu \nabla^2 + ((K + \mu/3) \nabla) \nabla \cdot ,$$

subject to the applicable boundary conditions, where ρ is the density, and K and μ are the bulk and shear moduli, respectively [19]. Unlike acoustic waves in air and flexural waves in plates, which are scalar waves, elastic waves are vector quantities, and satisfy a distinct wave equation from those describing acoustic or flexural waves.

Elastic wave solutions may be written as expansions in monochromatic plane waves,

$$\boldsymbol{\xi}(\mathbf{x}, t) = e^{j(\mathbf{k} \cdot \mathbf{x} - \omega t)}$$

where \mathbf{k} is a wave vector pointing in the direction of propagation, and ω is angular frequency. These may be decomposed into components transverse or parallel to the direction of propagation, $\hat{\mathbf{k}}$, respectively corresponding to shear $\boldsymbol{\xi}_T(\mathbf{x}, t)$ and compression $\boldsymbol{\xi}_L(\mathbf{x}, t)$ plane wave components. Their dispersion relations yield wave speeds $c_T = \sqrt{\mu/\rho}$ and $c_L = \sqrt{(K+4\mu/3)/\rho}$. Near the surface of a solid medium, boundary modes, such as Rayleigh or Love surface waves, mix bulk, shear, and compression wave components. Such boundary modes attenuate exponentially with depth, z , over a distance on the order of one wavelength, $\lambda = 2\pi/k$. They travel at speeds that are typically on the order of the shear wave speed [19]. At tactile frequencies ($f < 1000$ Hz), the contribution of compression waves (which travel at higher speeds) can be neglected.

Viscoelastic media exhibit frequency-dependent energy absorption and frequency-dependent speeds, $c(f)$ [19], [20], imparting them with complex wavenumbers, $k = k_1 + i\delta$. This causes monochromatic plane waves to decay with increasing distance, $\boldsymbol{\xi} \propto \exp(-a|\mathbf{x}|)\exp(j(\mathbf{k}\mathbf{x} - \omega t))$, where a is the absorption coefficient.

A. Driven Elastic Waves

Driven elastic waves $\boldsymbol{\xi}(\mathbf{x}, t)$ (solutions to Eq. 1) can be decomposed into responses in each spatial direction β , at remote positions \mathbf{x} , and at times t , to unit impulsive forces, $f_\delta(\mathbf{x}, t) = \delta(\mathbf{x} - \mathbf{y})\delta(t - s)$, delivered in directions α , at positions \mathbf{y} , and at times s . These responses are given by (causal, tensorial) Green's functions $g_y^{\alpha\beta}(\mathbf{x}, t - s)$, satisfying

$$L g_y^{\alpha\beta}(\mathbf{x}, t - s) = \delta(\mathbf{x} - \mathbf{y}) \delta(t - s) \delta^{\alpha\beta}. \quad (2)$$

An arbitrary driving force $\tilde{\mathbf{f}}(\mathbf{x}, t) = \mathbf{f}(t) \delta(\mathbf{x} - \mathbf{y})$ applied at position \mathbf{y} , elicits a wave field

$$\begin{aligned} \boldsymbol{\xi}^\beta(\mathbf{x}, t) &= \sum_{\alpha=1}^3 \int_{\Omega} d^3 y \int_{\mathbb{R}} ds g_y^{\alpha\beta}(\mathbf{x}, t - s) f^\alpha(s) \delta(\mathbf{x} - \mathbf{y}) \\ &= \sum_{\alpha=1}^3 g_y^{\alpha\beta}(\mathbf{x}, t) * f^\alpha(t) \end{aligned} \quad (3)$$

where Ω is the spatial domain and $*$ is convolution in time.

B. Time-Reversal Focusing in Elastodynamic Media

Our goal is to focus waves at arbitrary locations in the medium using actuators at locations \mathbf{y}_i , $i = 1, 2, \dots, N$. For time reversal (TR) focusing, we first measure $g_{\mathbf{y}_i}^{\alpha\beta}(\mathbf{x}_0, t)$ for each α and β , for each source location \mathbf{y}_i , and for each focal point \mathbf{x}_0 . We define a time-dependent driving force signal $\mathbf{f}_{\mathbf{y}_i}(t)$ at each source by convolving any time-varying excitation signal $u(t)$ with the corresponding time-reversed Green's function,

$$f_i^{TR}(t) = g_{\mathbf{y}_i}^{\alpha\beta}(\mathbf{x}_0, T - t) * u(t). \quad (4)$$

The wave field generated by the array of α -direction sources at positions \mathbf{y}_i , is given by

$$\boldsymbol{\xi}^\beta(\mathbf{x}, t) = \sum_{i=1}^N [g_{\mathbf{y}_i}^{\alpha\beta}(\mathbf{x}, t) * g_{\mathbf{y}_i}^{\alpha\beta}(\mathbf{x}_0, T - t)] * u(t) \quad (5)$$

where β is a wave field component direction. At the focal point, $\mathbf{x} = \mathbf{x}_0$, each factor in square brackets is the autocorrelation, $R_i(t - T)$, of $g_{\mathbf{y}_i}^{\alpha\beta}(\mathbf{x}_0, t)$, which attains a maximum at time $t = T$. Under mild assumptions (e.g., sufficiently large decay time and modal density) their sum approximates, up to a scale factor, a Dirac impulse, $\delta(t - T)$, in the β -direction, so that $\boldsymbol{\xi}^\beta(\mathbf{x}_0, t) \approx c u(t)$, where c is a constant. For each actuator, this occurs only at the focal point, \mathbf{x}_0 . The wave field achieves a spatial maximum at $\mathbf{x} = \mathbf{x}_0$ and $t = T$, with a focal width, d , that satisfies a Rayleigh criterion, $d > \lambda_m/2$, where λ_m is smallest wavelength signal component transmitted to the focus. TR focusing in heterogeneous media can yield even sharper focusing [21], underlining the robustness of this approach.

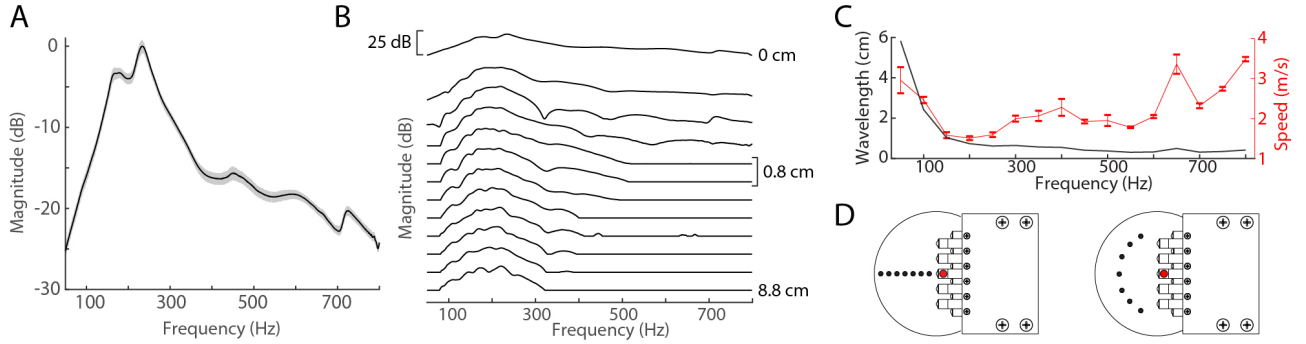


Fig. 2: A) The actuator frequency responses when driving the medium were similar for all actuators (grey outline: ± 1 standard error). B) Transfer functions from the front-center actuator signal to the evoked wave velocity in the medium at each of 12 increasing distances (panel D, left). The usable bandwidth was several hundred Hz at all distances, and was centered near 200–250 Hz. High frequencies attenuated faster with distance, reflecting frequency-dependent damping. C) The frequency dependent wave speed $c(f)$ was between 0.5 and 3.5 m/s. This implied effective wavelengths $\lambda(f)$ of 0.5 to 4 cm. Excluding frequencies at which waves were highly attenuated, the smallest wavelength was about 1 cm. D) Measurement positions for the transfer function measurements (left panel) and speed measurements (right panel).

An optimal TR focusing of elastic wave energy would use the actuators to drive all three vector components of displacement, and would sense the response in three directions at the focus. For each source and focus, this data would yield nine components of the Green's tensor, $g_{y_i}^{\alpha\beta}(\mathbf{x}_0, t)$. To make optimal use of this information would require solving a matrix deconvolution problem. In many practical cases [14], uniaxial focusing may be used, reducing complexity. We adopt this strategy here. Uniaxial TR focusing is based on one Green's function component per source, corresponding to one actuation direction, and one response direction (i.e., $g_{y_i}^{\alpha\beta}(\mathbf{x}_0, t)$, with both α and β indexing the direction normal to the medium surface for our device). Such a configuration yields TR focusing along the sensed axis at \mathbf{x}_0 , with residual energy transmitted to the orthogonal axes. A full discussion of elastic wave focusing, including boundary mode conversion and modal density, would exceed the scope of this paper.

IV. EMPIRICAL SYSTEM CHARACTERIZATION

We characterized the propagation of driven waves in our device using full-field optical vibrometry and signal processing, and we used the results to compute Green's functions for use in TR focusing at locations on the surface of the gel medium.

A. Apparatus

The device platform was bolted firmly to a vibration isolated optical table during the experiments. A scanning laser doppler vibrometer (Ometron, model 8330), positioned 50 cm above the surface of the elastomer captured the velocity of normal displacements of the medium that were excited by the actuators. Analog signals from the vibrometer were captured via an audio interface (MOTU, model 624, 48 kHz sampling rate, 24 bits). Output from the same interface controlled the laser position via custom software. The actuators were controlled with signals from a PC as described in Section II (Fig. 1B). A trigger signal from the

piezo amplifier ensured accurate synchronization during data capture.

B. Elastodynamic Response

To characterize the actuator response, we measured the normal velocity at the actuator driving point on the medium. The response (Fig. 2A) was similar for all actuators, exhibiting a broad resonance near 250 Hz, with a usable bandwidth extending from about 70 to 700 Hz.

We characterized the response produced by the center-front actuator to positions at 12 distances along the center of the medium surface, at 8 mm intervals (Fig. 2B). Higher frequency components generally attenuated faster with distance, reflecting frequency-dependent damping (Sec. III). The usable transmitted bandwidths decreased from about 600 Hz to 300 Hz with increasing distance.

We measured uniaxial Green's functions, i.e., impulse responses from each i th actuator to each focus position on the medium's surface. We obtained these as inverse Fourier transforms of the corresponding transfer functions, i.e., $g_{y_i}(\mathbf{x}_0, t) = \mathcal{F}^{-1}\{G_{y_i}(\mathbf{x}_0, \omega)\}$, with $G_{y_i}(\mathbf{x}_0, \omega) = V(\mathbf{x}_0, \omega)/A_i(\omega)$. Here, $V(\omega)$ and $A_i(\omega)$ were the Fourier transforms of the wave field velocity $v(t)$ at the focal point and of actuator signal $a_i(t)$ at y_i , respectively. We computed the transfer functions using a frequency sweep and decorrelation method (sweep duration 15 seconds, bandwidth 50 Hz to 800 Hz) averaged over 4 trials. For each focus location \mathbf{x}_0 , this yielded 16 Green's functions, one for each actuator (Fig. 3A shows representative results).

C. Estimating Wave Speed and Wavelength

We estimated the frequency-dependent speed $c(f)$ of wave propagation by cross-correlation of bandlimited noise signals transmitted from one actuator (front-center unit) to 7 equidistant positions on the medium (Fig. 2C). The estimated speeds were 1.5 to 3.5 m/s (slightly lower than surface wave speeds in human skin [22]). From these values, we also estimated

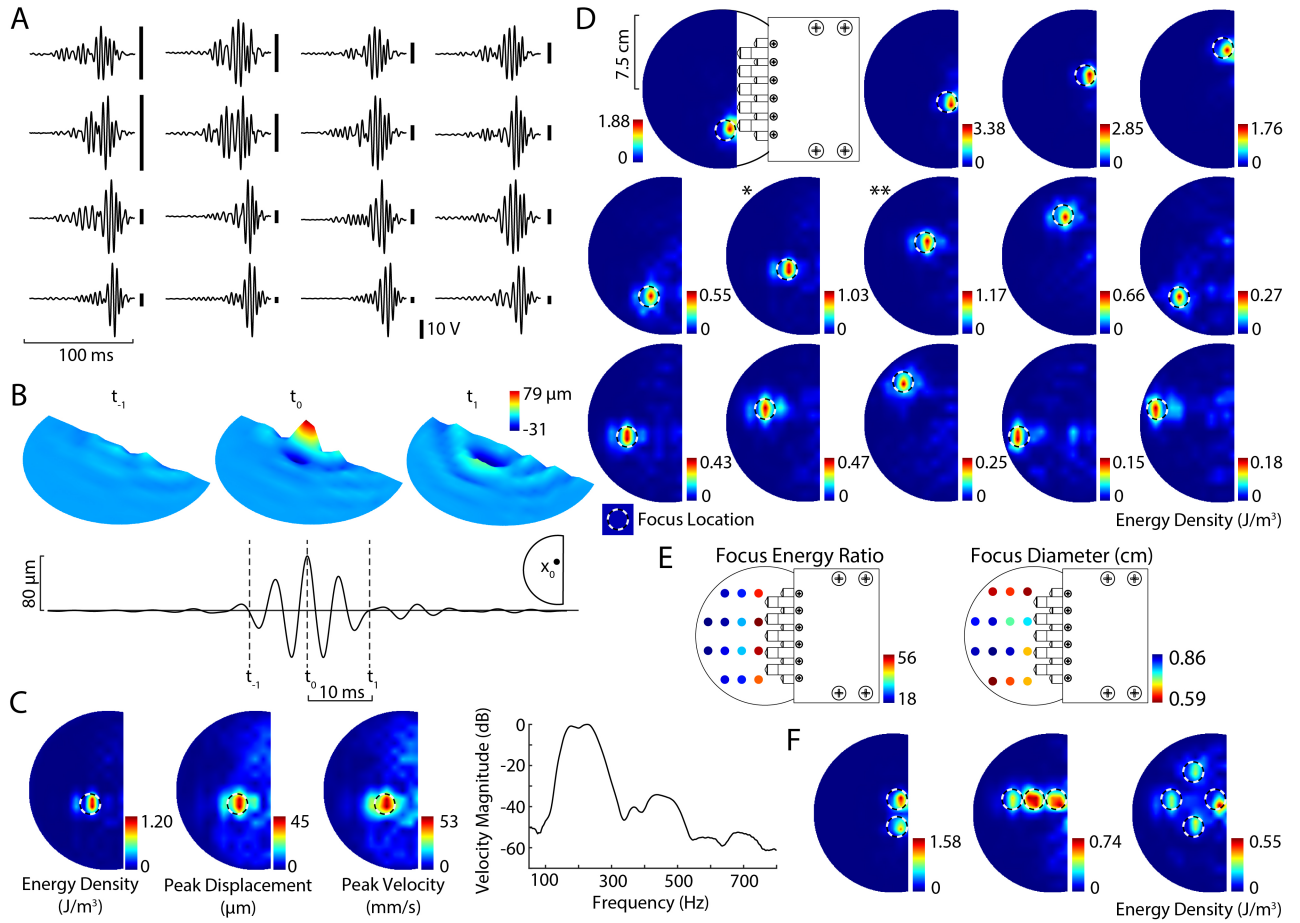


Fig. 3: A) Representative set of TR focusing driving signals $g_y(\mathbf{x}_0, T - t)$ for all 16 actuators, for one focal location. The voltage ranges for each signal, from ± 10 to ± 60 V, reflecting the relative contribution of each actuator. B) Measured time-resolved focused wave field (inset: focus location). At times $t_{-1} < T$ preceding focusing, the amplitude increases on the side closer to the actuators. At $t = T$, focusing is achieved, with a peak displacement of $80 \mu\text{m}$ at the focus location. For $t_{-1} > T$, the field quickly diffuses. The time-varying displacement at the focus location (lower panel) is a transient oscillation with center frequency near 200 Hz. C) Energy density, and short-time peak displacement and velocity, for a representative focus location. The velocity magnitude spectrum bandwidth at the focus extended from 100 Hz to >350 Hz. D) Energy density at the focus time, $t = T$, for each of 14 focal points. Most energy was confined near the focal point irrespective of the focus location. E) The focus energy ratio, r_E , was large, from 18 to 56. The effective focus diameter, d_f , averaged 0.72 cm. F) Results for simultaneous 2-, 3-, and 4-point focusing were similar to those obtained for single-point focusing (panel D).

the frequency-dependent spatial wavelength, $\lambda(f) = c(f)/f$, which ranged from 0.5 to 4 cm. The smallest wavelengths corresponded to high frequency components with low energy. Nonetheless, the results provide an estimate of the diffraction limited focal width as $d \approx 0.5$ cm, which could be considered to be a lower bound for our device, neglecting aperture size effects [14]. As the results presented below demonstrate, such a focal width was nearly attained in practice.

V. TR FOCUSING: IMPLEMENTATION AND EVALUATION

We implemented TR focusing for a variety of focus positions \mathbf{x}_0 by driving each i th actuator with time-reversed impulse responses $f_i(t) = g_{y_i}(\mathbf{x}_0, T - t) * u(t)$ (see Eq. 5), where $u(t)$ was a 2 ms white noise signal of constant amplitude. We evaluated the results via time-resolved measurements of the wave field normal velocity $v(\mathbf{x}, t)$ at 200

uniformly distributed surface locations, \mathbf{x} , averaged over 4 trials. We time-integrated the measured velocity to obtain the wave field normal displacement, $\xi(\mathbf{x}, t)$. We also computed short-time RMS averages of displacement $\xi_{RMS}(\mathbf{x})$, velocity $v_{RMS}(\mathbf{x})$, and energy density $E_{RMS}(\mathbf{x})$, with energy density given by $E_{RMS}(\mathbf{x}) = \frac{1}{2}\rho v_{RMS}(\mathbf{x})^2$, where $\rho = 925 \text{ kg/m}^3$ is the mass density of the gel medium. In order to assess the quality of focusing, we selected 14 focus locations distributed throughout the surface. We computed the area, A_f , within a contour beyond which the wave field energy at the focus time attenuated by one-half, and computed an effective diameter as the diameter $d_f = 2\sqrt{A_f/\pi}$ of a disc with equivalent area. We also computed the focus energy ratio, r_E , given by the ratio of the mean RMS energy density, $E_{RMS}(\mathbf{x})$, inside and outside the focus area at the focus time.

A. Results

The TR wave field attained maximum displacement at the focus position, \mathbf{x}_0 , for time $t = T$, consistent with theoretical predictions (Fig. 3B). Until times $t < T$, the field increased in amplitude on the side of the focus proximal to the array, and after time $t > T$ it rapidly diffused. The focused wave field displacement at $t = T$ reached nearly $100 \mu\text{m}$, and the maximum displacement was greater than $25 \mu\text{m}$ for all focus locations. For example, at the focus location shown in Fig. 3B, the displacement reached $79 \mu\text{m}$. Energy in the signal at the focus was centered broadly near a frequency of $f = 200 \text{ Hz}$ (Fig. 3C). Displacements of this magnitude and frequency would be easily perceived by users. For all 14 focus locations, at $t = T$, the great majority of the energy density in the wave field was confined near the focus location (Fig. 3D). The effective focal diameter, d_f , averaged 0.72 cm , and was less than 0.86 cm for all focus locations (Fig. 3E). This is only slightly larger than our estimate ($d \approx 0.5 \text{ cm}$) for the Rayleigh diffraction limit (Sec. IIIB and IVC). The focus energy ratio, r_E , was between 18 and 56 for all focal locations, indicating that most of the wave field energy was concentrated near the focus location at $t = T$. These results were obtained for conservative operating parameters in which the driving signal voltages were well within a range of $\pm 60 \text{ V}$. None approached amplifier or actuator limits. The residual unfocused energy outside the focal region was largest for focal locations near the distal edge of the surface, which could be due to their distance or to boundary effects.

B. Results: Multi-Point TR Focusing

Because of the small magnitude of the wave field oscillations relative to the characteristic dimensions (e.g., the 1 cm thickness of the medium), wave propagation in this regime can be regarded as very nearly linear [19]. Linearity implies that focused wave fields may be superimposed by additive combination of their driving signals. For each i th actuator, we computed a weighted sum of our single-point time-reversal filters, $g_y(\mathbf{x}_0, T - t)$, for multiple focus locations, \mathbf{x}_0 . We performed this for combinations of 2, 3, or 4 different focus locations. Informed by the results from single-point focusing, we adjusted the relative amplitudes for each focal point by weighting the sum appropriately. This ensured that the amplitudes at each focal point were similar.

The results show that the wave field was simultaneously focused at the intended locations, with most energy concentrated in the vicinity of each of the multiple foci (Fig. 3F). During multi-point focusing, the actuator energy was distributed among multiple focal regions. Nonetheless, near the focus time, the maximum energy density at each focal location during 2 and 3 point focusing was generally similar in magnitude to, if slightly lower than, the values we observed during single-point focusing at the same locations (Fig. 3D). For four point focusing, the maximum energy density was between 25% and 40% as large. The focal widths were qualitatively similar in size to what we observed for single point focusing. These findings demonstrate the effec-

tiveness of our method for multi-point tactile feedback. Our user evaluation, described next, provides further evidence.

VI. PERCEPTION: SINGLE- & MULTI-POINT FOCUSING

We investigated the perception of localized tactile feedback in two experiments. In the first, participants performed a binary discrimination between stimuli produced via single-point focusing to one of two locations (denoted by * and ** in Fig. 3D), and in the second, they performed a ternary discrimination between stimuli presented at either location or simultaneously to both of them. Ten participants volunteered for and participated in both experiments (ages 22 to 33, 3 female, 7 male). None reported any disorders affecting touch sensation. Participants gave their written, informed consent and the experiment was approved by the human subjects research committee of our institution.

Stimuli in the experiment consisted of single- and multi-point focused wave fields rendered, as described in the foregoing sections, using an excitation signal $u(t)$ (see Eq. 5), which we designed as a short train of ten 2 ms white noise signals with unit amplitude, spaced by pauses of 20 ms . The driving voltages were similar to those shown in Fig. 3A, with peak voltages less than $\pm 60 \text{ V}$.

Participants were seated facing the Elastowave display during the experiment. Their left and right index fingers each touched the gel medium at axially symmetric locations 2.5 cm apart at a distance 4 cm from the array. Participants applied light (approx. 1 N) force which was not controlled by the experimenter. To mask any auditory cues, participants wore earplugs (rating: -33 dB) and circumaural headphones playing white noise. The experimenter was seated out of view of the participants. He operated the computer and recorded verbal responses from the participants.

In the first, single-point, focusing experiment, on every trial a stimulus was focused to a location beneath one of the two index fingers. Participants reported whether the stimulus was felt at the left or right location. Participants were free to request that a stimulus be repeated before providing their response. The multi-point experiment was identical in procedure, except that on each trial a stimulus was focused to a location beneath the left finger, right finger, or simultaneously at both. Participants responded indicating whether they felt the stimulus at the left location, right location, or both. For each participant the single point experiment lasted 20 trials, with 10 repetitions of “left” or “right” focused stimuli. The multipoint experiment consisted of 30 trials, with 10 repetitions of each of the three focused stimuli. In both experiments, the stimuli were in randomized order. Participants received no training prior to the experiment and no feedback during the experiment. All participants completed the first experiment followed by the second experiment. They provided brief written and verbal comments after the experiment.

A. Results

In the single-point experiment, every participant correctly identified the location of the stimulus on every trial, corre-

sponding to 100% accuracy. This was true for all trials for both the left- and right-focused stimuli. Chance performance would correspond to 50%. In the multi-point experiment, the responses were also generally very accurate. In this experiment, all participants correctly identified the stimulus location for trials in which stimuli were focused on the left (correct response rate of 100%). For stimuli focused on the right, 7 of 10 participants correctly identified the location on all trials. The remaining 3 participants each responded correctly on 80% to 90% of the trials. This yielded a median correct response rate of 100% across all participants for the “right” stimulus trials. For trials in which multi-point stimuli were presented simultaneously at both the left and right locations, the median performance was 90%. 2 of 10 subjects responded correctly on every such trial, while one of the 10 subjects performed at chance levels (3 of 10 correct; chance performance: 33%). Informally, based on participant comments and our own observations, the presentation of stimuli that were felt simultaneously at both fingers during the multi-point trials may have created confusion about what was felt, but further research would be needed to clarify this. In summary, the results indicate that both the single- and multi-point stimuli were perceived at the locations to which they were focused on the great majority of trials. All responses in the first experiment, and 91% of the responses in the second experiment identified the location of the focused stimuli correctly.

VII. DISCUSSION AND CONCLUSION

This paper introduced the Elastowave, a soft tactile interface that provides localized feedback via a deformable surface. We achieve this by exploiting mechanical transmission in the medium in order to focus elastic wave fields generated by a compact array of remotely-positioned actuators to small regions on the surface. Because this method enables the actuators to be positioned remotely, it preserves the ability of the soft medium to stretch and deform when touched. This work also introduced new variations on time-reversal focusing methods for elastodynamic waves in soft media. As our results demonstrate, these methods enable dynamic, localized rendering of single- or multi-point tactile feedback anywhere on the active area of the device. We demonstrated up to 4-point focusing, which is the largest number we attempted. The average effective focus width was 0.72 cm. This approached the Rayleigh diffraction limit, $d > 0.5$ cm, that we estimated based on our measurements.

The displacements that the device generates at the focal points are sizeable, reaching nearly 100 μm in magnitude, which is larger than the displacements generated by TR focusing in stiff plates. In our device, most of the energy in the focused signals lies in a frequency band near 200 Hz (Fig. 3C), well within the frequency range of greatest vibrotactile sensitivity. The low mechanical impedance of the gel medium ensures that the stimulus energy can be efficiently transmitted to a user’s finger. Indeed, in our experiments, users were able to perfectly discriminate brief, localized tactile stimuli during single-point focusing. They

were also able to accurately discriminate stimuli in a more complex task that involved both single- and multi-point foci. Informally, this task occasionally became confusing due to the simultaneity of the stimuli felt on different fingers during multi-point focusing.

Because our tactile display method is data-driven, rather than model-based, it was not essential that we select this particular geometry for the soft medium. Other complex or 3D shapes could be used. Soft media with different mechanical properties could also be used. The choice of medium will affect the wave transmission properties (Fig. 2), but the effects can be anticipated from theory (Sec. III). For example, selecting a material with greater elasticity or greater mass density will reduce the wave speeds, and hence wavelengths, which may enable finer focusing (other limitations notwithstanding). Our device used a compact array of 16 piezoelectric cantilever actuators which provided sufficient displacement and energy in the tactile frequency range. However, many other actuators could be utilized because the actuator response is accounted for in the time-reversed signal that satisfies the focusing condition. Other array configurations could also be employed.

We envision the Elastowave as a tactile interface providing input and output. While the work presented here primarily addresses the device design and tactile focusing (output) methods, many techniques could be used to sense user inputs. These include optical- and camera-based sensing within or external to the medium, integrated soft resistive sensing, capacitive sensing, or acoustic sensing methods. We have prototyped one approach, combining camera-based sensing with video projection (Fig. 1D). In a different embodiment, a video screen can be positioned below the gel medium in order to present visual feedback. Our device’s surface is semi-opaque, due to an optical treatment that we used in the vibrometry experiments, but the medium is otherwise transparent. Soft tactile touch screens could prove useful in many applications. We plan to investigate this in the future.

Future Opportunities

Soft surfaces and contacts are common in nature, in interpersonal touch, and in many designed artifacts. In industrial design, they are often used to improve comfort, aesthetics, or ergonomics. The work presented here could lead to soft tactile interfaces that could be integrated in many applications. These could include complex multitouch interfaces for augmented or mixed reality, in which touch feedback is mediated by sculpted or shape-changing soft interfaces, or, in simpler embodiments, soft handheld or panel-mounted controllers that can provide programmable tactile feedback at a few locations. Many other embodiments are possible. We envision new applications of such soft tactile interfaces in many arenas, including soft interfaces for expressive multimedia performance, soft interfaces for tactile communication, and programmable soft control panels for automotive cockpits.

ACKNOWLEDGEMENT

This work was supported by the US National Science Foundation (NSF-1628831, NSF-1623459, NSF-1751348) and by Facebook Reality Labs. We thank V. Hayward and T. Hachisu for discussion and A. Kawazoe for help in creating an interactive demonstration with the Elastowave.

REFERENCES

- [1] J. Jiao, D. Wang, Y. Zhang, D. Cao, Y. Visell, X. Guo, and X. Sun, “Detection and discrimination thresholds for haptic gratings on electrostatic tactile displays,” *IEEE Transactions on Haptics*, vol. 12, no. 1, pp. 34–42, 2018.
- [2] A. Girard, M. Marchal, F. Gosselin, A. Chabrier, F. Louveau, and A. Lécuyer, “Haptip: Displaying haptic shear forces at the fingertips for multi-finger interaction in virtual environments,” *Frontiers in ICT*, vol. 3, p. 6, 2016.
- [3] D. Leithinger, S. Follmer, A. Olwal, and H. Ishii, “Physical telepresence: shape capture and display for embodied, computer-mediated remote collaboration,” in *Proceedings of the 27th annual ACM symposium on User interface software and technology*. ACM, 2014, pp. 461–470.
- [4] N. Kastor, V. Vikas, E. Cohen, and R. D. White, “A definition of soft materials for use in the design of robots,” *Soft Robotics*, vol. 4, no. 3, pp. 181–182, 2017.
- [5] D. Rus and M. T. Tolley, “Design, fabrication and control of soft robots,” *Nature*, vol. 521, no. 7553, pp. 467–475, 2015.
- [6] H. A. Sonar and J. Paik, “Soft pneumatic actuator skin with piezoelectric sensors for vibrotactile feedback,” *Frontiers in Robotics and AI*, vol. 2, p. 38, 2016.
- [7] M. Zhu, T. N. Do, E. Hawkes, and Y. Visell, “Fluidic fabric muscle sheets for wearable and soft robotics,” *Soft Robotics*, (To Appear), 2019.
- [8] A. A. Stanley and A. M. Okamura, “Controllable surface haptics via particle jamming and pneumatics,” *IEEE Transactions on Haptics*, vol. 8, no. 1, pp. 20–30, 2015.
- [9] M. Matysek, P. Lotz, and H. F. Schlaak, “Tactile display with dielectric multilayer elastomer actuators,” in *Electroactive Polymer Actuators and Devices (EAPAD) 2009*, vol. 7287. International Society for Optics and Photonics, 2009, p. 72871D.
- [10] Y. Shao, S. Ma, S. H. Yoon, Y. Visell, J. Holbery, and T. Large, “Surfaceflow: Large area haptic display via compliant liquid dielectric actuators,” in *2020 IEEE Haptics Symposium (HAPTICS)*. IEEE, Submitted, 2020.
- [11] T. N. Do, H. Phan, T.-Q. Nguyen, and Y. Visell, “Miniature soft electromagnetic actuators for robotic applications,” *Advanced Functional Materials*, vol. 28, no. 18, p. 1800244, 2018.
- [12] S. Biswas and Y. Visell, “Emerging material technologies for haptics,” *Advanced Materials Technologies*, vol. 4, no. 4, p. 1900042, 2019.
- [13] A. Farooq, G. Evreinov, and R. Raisamo, “Evaluating different types of actuators for liquid screen overlays (Iso),” in *2016 Symposium on Design, Test, Integration and Packaging of MEMS/MOEMS (DTIP)*. IEEE, 2016, pp. 1–6.
- [14] M. Fink, “Time reversal of ultrasonic fields. i. basic principles,” *IEEE Transactions on Ultrasonics, Ferroelectrics, and Frequency Control*, vol. 39, no. 5, pp. 555–566, 1992.
- [15] A. J. Berkhouit, D. de Vries, and P. Vogel, “Acoustic control by wave field synthesis,” *Journal of the Acoustical Society of America*, vol. 93, no. 5, pp. 2764–2778, 1993.
- [16] M. R. Bai and Y. K. Tsai, “Impact localization combined with haptic feedback for touch panel applications based on the time-reversal approach,” *The Journal of the Acoustical Society of America*, vol. 129, no. 3, pp. 1297–1305, 2011.
- [17] C. Hudin, J. Lozada, and V. Hayward, “Localized tactile feedback on a transparent surface through time-reversal wave focusing,” *IEEE Transactions on Haptics*, vol. 8, no. 2, pp. 188–198, 2015.
- [18] T. Hoshi, M. Takahashi, T. Iwamoto, and H. Shinoda, “Noncontact tactile display based on radiation pressure of airborne ultrasound,” *IEEE Transactions on Haptics*, vol. 3, no. 3, pp. 155–165, 2010.
- [19] J. Achenbach, *Wave propagation in elastic solids*. Elsevier, 2012, vol. 16.
- [20] B. Dandu, Y. Shao, A. Stanley, and Y. Visell, “Spatiotemporal haptic effects from a single actuator via spectral control of cutaneous wave propagation,” in *2019 IEEE World Haptics Conference (WHC)*. IEEE, 2019, pp. 425–430.
- [21] M. Fink, “Time-reversal acoustics in complex environments,” *Geophysics*, vol. 71, no. 4, pp. SI151–SI164, 2006.
- [22] L. R. Manfredi, A. T. Baker, D. O. Elias, J. F. Dammann III, M. C. Zielinski, V. S. Polashock, and S. J. Bensmaia, “The effect of surface wave propagation on neural responses to vibration in primate glabrous skin,” *PLoS One*, vol. 7, no. 2, p. e31203, 2012.